Theor Chem Acc (2012) 131:1209
DOI 10.1007/s00214-012-1209-8

REGULAR ARTICLE

# Theoretical study on the structures and electronic properties of oligo(*p*-phenylenevinylene) carboxylic acid and its derivatives: effects of spacer and anchor groups

**Songwut Suramitr · Apipol Piriyagagoon · Peter Wolschann · Supa Hannongbua**

Received: 7 June 2011 / Accepted: 20 March 2012 / Published online: 7 April 2012


**Abstract** The structural parameters of oligo(*p*-phenylenevinylene)carboxylic acid ($OPV_3$–COOH) and its derivatives were optimized using the density functionals B3LYP, M06, M06-HF, M06-2X and the MP2 method on 6-31G(d) basis set level. The results show that the structure from B3LYP calculation is more planar than from M06, M06-2X, M06-HF, and MP2, respectively. The structures of $OPV_3$–COOH obtained from various methods were used to calculate the electronic properties by time-dependent density functional theory calculation with the TD-CAM-B3LYP/6-311G(d,p) including conductor polarizable continuum model solvation to compare with the experimental absorption bands of this molecule. The excitation energies from the coplanar structure using M06-2X/6-31G(d) (406 nm) are closer to the experimental absorption data (430 nm) than the data from geometries optimized by M06-HF/6-31G(d) (362 nm) and MP/6-31G(d) (382 nm). Therefore, in this study, the M06-2X/6-31G(d) method was selected to investigate the effects of spacers for the structures and the electronic properties of $OPV_3$–COOH and some derivatives. Spacer groups such as thiophene, dithiophene and vinylenethiophene linking between chromophore and the cyanoacrylic acid (–CNCOOH) anchor group can increase the electron transfer and expand the $\pi$-conjugated system to shift the absorption band into the visible light region. The more extended electron transfer and the red-shift of the absorption band for $OPV_3$–COOH and $OPV_3$–CNCOOH derivatives are desirable for absorbing sunlight and good employing as photo-sensitizer in dye-sensitized solar cell. Thiophene ($OPV_3$–Th–CNCOOH), dithiophene ($OPV_3$–diTh–CNCOOH) and vinylenethiophene ($OPV_3$–viTh–CNCOOH) as spacer lead to the expansion of the $\pi$-conjugated system and to bathochromically shifted absorption spectra. Therefore, the modeling of side chain, spacer and anchor group in this study suggests new sensitizer compounds that enhance the efficiency of electron transfer and absorption of the sunlight for new synthetic materials.

**Keywords** Dye-sensitized solar cell (DSSC) · Oligo(*p*-phenylenevinylene) carboxylic acid · Time-dependent density functional theory (TDDFT)

S. Suramitr (✉) · A. Piriyagagoon · S. Hannongbua
Department of Chemistry, Faculty of Science, Kasetsart University, Bangkok 10900, Thailand
e-mail: fsciswsm@ku.ac.th

S. Suramitr · A. Piriyagagoon · S. Hannongbua
The Center of Nanotechnology KU, Kasetsart University, Bangkok 10900, Thailand

P. Wolschann
Institute for Theoretical Chemistry, University of Vienna, Währinger Straße 17, 1090 Vienna, Austria

## 1 Introduction

The basis of sunlight energy absorption is the use of silicon-containing materials as semiconductors in solar cells. But the production of these semiconductors is expensive so that scientists try to develop dye-sensitized solar cells (DSSCs) [1, 2]. The first DSSCs were investigated by Regan and Grätzel et al. [2, 3] in 1991. The production of DSSCs is less expensive and the efficiency is close to the silicon-containing compound solar cells. The disadvantage of DSSCs is the poor stability at high temperatures and the short usage time. Therefore, the design of new DSSCs with enhanced properties, higher stability and longer usage time was the topic of further research. The most popular dyes

that scientists developed are Ru(II) complexes, such as N3 ([Ru-(dcbpyH$_2$)$_2$(NCS)$_2$]), N719 ((Bu$_4$N)$_2$[Ru(dcbpyH)$_2$(NCS)$_2$]), because these are the best metal organic complex dyes [4]. The performance attained in solar-to-electric conversion efficiency of Ruthenium Dye N3 is 11 % [5]. Although the metal dye sensitizers as DSSCs have high extinction coefficients and good efficiency, the danger of environmental pollution exists. Therefore, there is also increasing interest in metal-free organic dyes [6] as new alternative sensitizers due to their many fold advantageous features, such as high molar extinction coefficients, easily modified molecular structure and relatively low cost materials. In general, such compounds possess both $\pi$–$\pi^*$ and charge-transfer absorption bands in the electronic spectra, which correlates to the good electron injection efficiency in DSSCs. Power conversion efficiencies up to $\sim$9 % have been achieved for DSSCs based on metal-free dyes [7–9]. Moreover, highly impressive the power conversion efficiency (PCEs) ($\sim$10 %) with excellent stability was also reported in very recent publications of Wang et al. [10].

Hal et al. [11] reported the interaction of an acid-functionalized, oligo(*p*-phenylenevinylene)-carboxylic acid (OPV$_3$–COOH) with nanocrystalline TiO$_2$ studied as a model for semiconducting polymer–inorganic material hybrid solar cells. Photoluminescence quenching and near steady-state photo-induced absorption spectroscopy demonstrate that an efficient forward photoinduced electron transfer occurs from OPV$_3$–COOH to TiO$_2$. However, a DSSC using OPV3–COOH comparable to that observed for a Ru dye-sensitized cell demonstrates that not only the charge generation is efficient, but also the collection efficiency is high. Recently, Kim and coworkers [12] have synthesized three organic sensitizers containing bis-dimethylfluorenyl amino groups and a cyanoacrylic acid acceptor bridged by a *p*-phenylene vinylene unit. They found that the PCE was quite sensitive to the length of bridged phenylene vinylene groups. The maximum power conversion efficiency of JK-59 reached 7.02 %. These oligo(*p*-phenylene vinylenes) are being actively investigated for use in solar cells due to their stability and high luminescent efficiency [12–14]. In this investigation, we applied density functional theory (DFT) calculations to obtain some guidance for the synthesis of new materials for DSSCs.

A quantitative understanding of molecular electronic excited states is important in many disciplines, including spectroscopy, photochemistry and the design of optical materials [15–28]. The prediction or interpretation of the discrete part of the spectrum is a demanding task for theoretical methods, especially for medium- and large-sized molecules. Quantum chemical calculations are applied to obtain geometrical parameters as well as electronic properties. Herein, we report the investigation of both spacer and anchor groups (Fig. 1) on the structures and the electronic properties of OPV$_3$–COOH and OPV$_3$–CNCOOH derivatives by quantum chemical calculations. From the ground-state geometries, electronic transitions were achieved by time-dependent density functional theory (TD-DFT) [29–32] calculations with the PBE0 functional [33, 34] and Coulomb-attenuated hybrid exchange–correlation functional (CAM-B3LYP) [35, 36]. These information leads to the new design of sensitizers for DSSCs. In this study, electronic properties, charge transfer, and the effect of spacers and anchors group of OPV$_3$–COOH and its derivatives were theoretically investigated.

## 2 Computational details

### 2.1 Ground-state calculations

The structures of OPV$_3$–CNCOOH derivatives were obtained by introducing spacer groups between the chromophore group and the anchor group. The spacer groups consist of thiophene (OPV$_3$–Th–CNCOOH), dithiophene (OPV$_3$–diTh–CNCOOH) and vinylenethiophene (OPV$_3$–viTh–CNCOOH) (shown in Fig. 1). The methoxy side chain groups are used instead of alkoxy group of OPV$_3$–COOH for reducing the computational time. This is because reports suggest that substituents at the alkoxy group play an important role in the thermal stability and solubility but do not affect the electronic properties of compounds [37]. The structures were fully optimized by using DFT method with hybrid functionals [38–42] (B3LYP, M06, M06-HF, M06-2X) and second-order Moller–Plesset Perturbation Theory (MP2) [43] methods at 6-31G(d) basis set level [44], respectively. The Berny analytical gradient method was used for the optimizations. The requested convergence on the density matrix was $10^{-8}$, and the threshold values for the maximum force and the maximum displacement were 0.00045 and 0.0018 a.u., respectively. All calculations were implemented in Gaussian 09 [45]. These structures were confirmed to be local minima by the vibrational frequency analysis. The structural results such as bond lengths, bond angles and bond torsions are compared to X-ray crystallography data [46] with the mean relative errors defined as

$$\sum_{i=1}^{n} \frac{|X_{\mathrm{Cal}} - X_{\mathrm{Exp}}|}{|X_{\mathrm{Exp}}|} \Big/ n \qquad (1)$$

For conjugated molecular system, the structures were often described by bond length alternation (BLA) [47, 48], which is defined as differences in lengths between single and double bonds. In this work, BLA for the

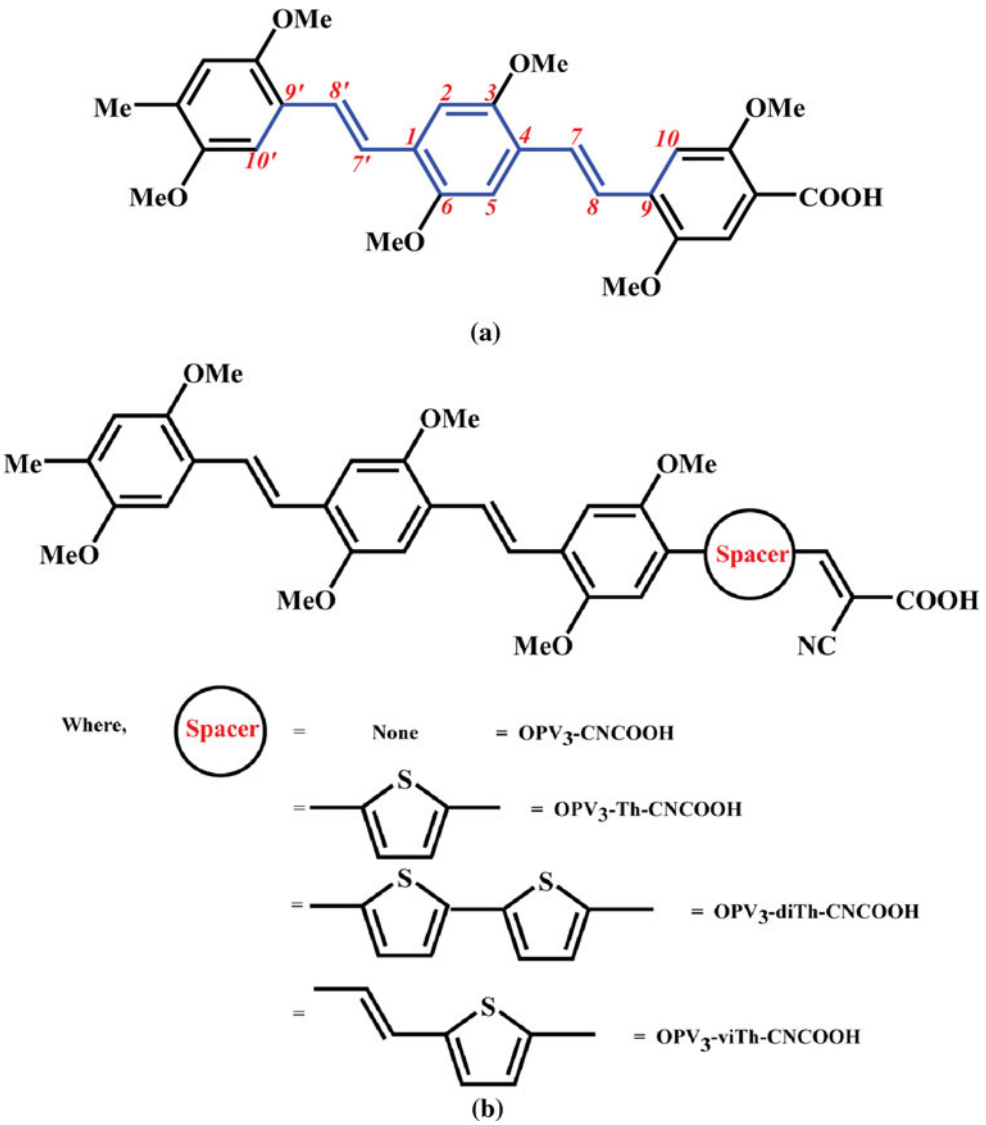


**Fig. 1** Schematic representation of (**a**) $OPV_3$–COOH and (**b**) $OPV_3$–CNCOOH derivatives. Labeled numbers are for the notation in this study

phenylenevinylene subunit of $OPV_3$–COOH and $OPV_3$–CNCOOH derivatives were defined as follow

$$\begin{aligned}\mathrm{BLA} = {} & 2[(\mathrm{C2}-\mathrm{C3}) + (\mathrm{C5}-\mathrm{C6})] - [(\mathrm{C1}-\mathrm{C2}) \\ & + (\mathrm{C3}-\mathrm{C4}) + (\mathrm{C4}-\mathrm{C5}) + (\mathrm{C1}-\mathrm{C6})] \\ & + [(\mathrm{C4}-\mathrm{C7}) + (\mathrm{C8}-\mathrm{C9})] - 2(\mathrm{C7}-\mathrm{C8}) \end{aligned} \quad (2)$$

## 2.2 Excited state calculations

The calculations of the excitation energies were then performed based on the ground-state geometries. Methods and basis set dependence of excitation energies calculated with TD-DFT were also investigated for $OPV_3$–COOH and $OPV_3$–CNCOOH derivatives, including functional oligomers with spacer and anchor groups. The electronic transitions were achieved by the PBE0 functional and CAM-B3LYP functional to investigate the electron excitation absorption wavelengths, and energy states. The CAM-B3LYP functional has been demonstrated to provide good results for Rydberg transitions and excitations in small molecules as well as for intermolecular charge-transfer transitions [49, 50]. This new density functional has recently been developed specifically to overcome former limitations in charge-transfer transitions, and it has been shown to predict molecular charge transfer accurately. The calculations were used as the basis of TD-DFT calculations on the $S_0$ to $S_1$, $S_2$, $S_3$, $S_4$ and $S_5$ states of each molecule using 6-311G(d,p) basis set [51] in toluene solvent to investigate the chain length dependence of the vertical excitation energies of $OPV_3$–COOH and $OPV_3$–CNCOOH derivatives. Indeed, the basis sets additionally provide diffuse basis functions, which allow for a better representation of the tails of the wave functions. However, sufficiently converged results were obtained with the

**Table 1** Structural parameters of $OPV_3$–COOH obtained from full optimization by B3LYP, M06 functionals and MP2 at 6-31G(d) level of basis set (bond lengths in Ångstrom, angles in degrees)

| Structural parameters | B3LYP/6-31G(d) | M06/6-31G(d) | M06-HF/6-31G(d) | M06-2X/6-31G(d) | MP2/6-31G(d) | X-ray |
|---|---|---|---|---|---|---|
| Bond length | | | | | | |
| C1–C2 | 1.395 | 1.400 | 1.395 | 1.398 | 1.404 | 1.380 |
| C2–C3 | 1.395 | 1.387 | 1.392 | 1.388 | 1.394 | 1.390 |
| C3–C4 | 1.395 | 1.412 | 1.401 | 1.407 | 1.412 | 1.390 |
| C4–C5 | 1.395 | 1.402 | 1.396 | 1.399 | 1.405 | 1.400 |
| C5–C6 | 1.395 | 1.386 | 1.391 | 1.387 | 1.394 | 1.340 |
| C6–C1 | 1.395 | 1.412 | 1.403 | 1.408 | 1.412 | 1.370 |
| C4–C7 | 1.540 | 1.452 | 1.479 | 1.463 | 1.460 | 1.470 |
| C7–C8 | 1.326 | 1.348 | 1.336 | 1.342 | 1.353 | 1.320 |
| C8–C9 | 1.540 | 1.455 | 1.481 | 1.465 | 1.461 | 1.470 |
| Bond angle | | | | | | |
| C3–C4–C7 | 120.0 | 119.5 | 119.1 | 119.6 | 119.6 | 125.3 |
| C4–C7–C8 | 122.7 | 126.8 | 124.2 | 125.8 | 124.4 | 125.3 |
| Torsion angle | | | | | | |
| C5–C4–C7–C8 | −30.3 | −14.6 | −28.0 | −15.7 | −27.3 | −18.0 |
| C7–C8–C9–C10 | 30.0 | 16.4 | 29.7 | 18.6 | 29.0 | 18.0 |
| H–bond | | | | | | |
| R1(O–H) | 2.585 | 2.320 | 2.394 | 2.329 | 2.422 | 2.420 |
| R2(O–H) | 2.582 | 2.336 | 2.434 | 2.330 | 2.420 | 2.450 |
| R3(O–H) | 2.585 | 2.278 | 2.415 | 2.322 | 2.406 | 2.390 |
| R4(O–H) | 2.582 | 2.325 | 2.430 | 2.332 | 2.417 | 2.460 |
| Relative error | 0.020 | 0.010 | 0.012 | 0.010 | 0.013 | – |
| BLA | 0.428 | 0.131 | 0.259 | 0.182 | 0.158 | 0.22 |

BLA and the mean relative error values are also listed

valence double-zeta quality with polarization functions basis sets in close agreement with many previous studies for considering the computational costs and consistency [52].

The conductor polarizable continuum model (CPCM) is also applied [53–56] taking into account the solvation effect. Singlet electronic spectra, density of state (DOS) and electron polarizations between ground and excited states were obtained from TD-DFT data.

## 3 Results and discussion

### 3.1 Method validation

#### *3.1.1 The comparison of computed ground-state geometry parameters obtained from different theoretical methods with the experimental data for $OPV_3$–COOH*

The optimized geometrical parameters using DFT method with hybrid functionals (B3LYP, M06, M06-HF, M06-2X) and MP2 method are presented in Table 1. The calculated parameters, bond lengths and bond angles, agree with the X-ray crystallographic data reported by Stalmach et al. [46]. To simplify the presentation of the geometries of the phenylene ring of $OPV_3$–COOH (Fig. 1), for the bond lengths, only average values are given. From the mean relative errors (0.020, 0.010, 0.012, 0.010 and 0.013) and the BLA (0.428, 0.131, 0.259, 0.182 and 0.158), it can be see that the optimized ground-state geometries obtained from B3LYP, M06, M06-HF, M06-2X and MP2, respectively, are in good agreement with the crystallographic data. The key parameters become closer to the experimental results with the 6-31G(d) basis set. The bond angles C3–C4–C7 and C4–C7–C8 in B3LYP/6-31G(d) and M06 functionals optimized geometries (about ∼120° and ∼120°) are similar and close to crystallographic data (about ∼125.3°), but the torsion angles C4–C5–C7–C8 and C7–C8–C9–C10 are significantly different. Considering the torsion angles from the B3LYP method (−30.3° and 30.0°) and M06 functional, the $OPV_3$–COOH structure is non-planar with both phenylene ring oppositely twisted within ∼30° apart from the planar configuration. For the solid state, both the non-planar (Fig. 2) and the planar structures of $OPV_3$–COOH should be considered. The different ground-state geometries obtained from different

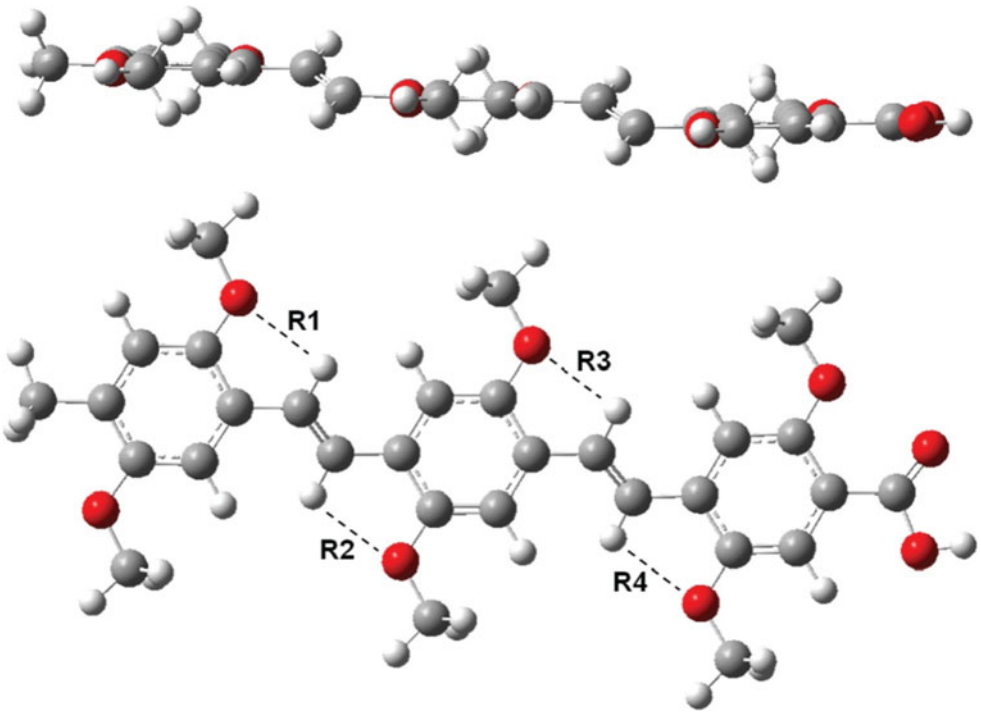


**Fig. 2** Side view of $OPV_3$–COOH optimized structure. Non-planar configuration and weak intramolecular hydrogen bonding between oxygen atoms on alkoxy groups and hydrogen atoms at vinylene linkage in $OPV_3$–COOH

theoretical methods are noteworthy because the accuracy of the structure prediction leads to reliable property calculations. The $OPV_3$–COOH structure is therefore optimized using a higher level method of calculation such as MP2.

In Table 1, $OPV_3$–COOH geometries obtained from B3LYP, M06, M06-HF, M06-2X and MP2/6-31G(d) are given. The presence of four intramolecular hydrogen bonds between oxygen atom of substituents and the hydrogen atoms at the vinylene linkage (O1–H1, O2–H2, O3–H3 and O4–H4) (Fig. 2) is shown. The hydrogen bond average distances between the oxygen atoms of the alkoxy groups and the hydrogen atoms at vinylene linkages are 2.58, 2.30 and 2.42 Å from geometries optimized using B3LYP, M06 functionals and MP2, respectively. The results from three optimized structures indicate that the average distance of R(O–H) of about 2.40 Å is in the range of weak intramolecular hydrogen bonds. This similar observation is supported by the work of Stalmach et al. [46] where it was found that the distance between oxygen and hydrogen atoms reaches values above 2.4 Å in X-ray structures of several compounds for 2,5-dialkoxy-substitued PPVs. Similar observations were reported by Suramitr et al. [57], where it is indicated that in $OPV_3$–COOH intramolecular hydrogen bonding between oxygen atom of alkoxy group and hydrogen atom at vinylene linkage occurs. Due to the steric effect, the structures are non-planar. The M06-HF, M06-2X and MP2 optimized geometrical parameters for $OPV_3$–COOH (bond lengths, bond angles, torsion angles) including BLA and relative error values are presented in Table 1. It is found that the mean relative error of bond lengths ($\sim$0.010), bond angles ($\sim$120) and the BLA ($\sim$0.2) of the phenylenevinylene ring is close to X-ray crystallographic data. Therefore, in next section, electronic transitions of $OPV_3$–COOH were investigated to confirm the better configuration structure for ground-state geometry optimizations from different methods. It is indicated that M06-HF, M06-2X and MP2 methods are reliable for the calculation of the ground-state geometries of $OPV_3$–COOH and its derivatives. The M06 families of functionals are highly parameterized forms of standard metahybrid approximations and dispersion correcting atom-centered one-electron potentials. These approaches are recommended that the dispersion energy is highlighted for study in conformational problems [58].

### *3.1.2 Comparison of the electronic transitions calculated from ground-state geometries optimized with M06-HF, M06-2X functionals and MP2 method*

Electronic transitions of $OPV_3$–COOH derivatives were investigated to get information about the applicability of various methods. Excitation energies and oscillator strengths for the transition from ground state ($S_0$) to $S_1$, $S_2$, $S_3$ and $S_4$ states of $OPV_3$–COOH were calculated using the TD-DFT method including the solvation effect of toluene at the PBE0 and CAM-B3LYP with 6-311G(d,p) level, using M06-HF, M06-2X, and MP2 optimized ground-state structures. PCM employs the parameters and iterative calculations to take the toluene solvation effect into account. Comparisons of the predicted values of the

absorption band of this molecule in toluene [11] were made in Table 2. TD-PBE0 and TD-CAM-B3LYP calculations on all ground-state geometries are used to predict the oscillator strengths. Calculations of electronic transition lead to two important transitions: $S_0 \rightarrow S_1$ and the $S_0 \rightarrow S_4$ states. It is found that the $S_0 \rightarrow S_1$ transition corresponding to the excitation from the HOMO to the LUMO is dominant as indicated by large oscillator strengths ($f \approx 1.5$), while other $S_0 \rightarrow S_4$ states were found to be relevant in the energy region of the UV absorption ($f \approx 0.1$). Therefore, in our study, only the calculated $S_0 \rightarrow S_1$ excitations are investigated to correspond to the maximum absorption peak observed in experimental UV–vis spectrum.

In Table 2, the absorption wavelengths of the $S_0 \rightarrow S_1$ transition of $OPV_3$–COOH structures obtained from TD-PBE0 based on M06-HF, M06-2X and MP2 ground-state geometries are 425 (2.92 eV), 468 (2.65 eV) and 445 nm (2.78 eV), respectively. The TD-PBE0 values are in good agreement with the observed value. However, the DSSC systems investigated clearly exhibit a charge-transfer character. For this specific subset, it appears that TD-PBE0 is generally adequate, but for states featuring a significant charge-transfer character, for which TD-CAM-B3LYP has the edge [59, 60].

The CAM-B3LYP was also examined for taking account of the long-range corrections for describing this

**Table 2** Calculated transitions for $OPV_3$–COOH using PCM-TD-DFT, PBE0 and CAM-B3LYP functionals at 6-311G(d,p) basis set, compared to the experimental absorption wavelengths in the toluene solvent

| State | Eex (nm) | Eex (eV) | $f$ | Transition characters |
|---|---|---|---|---|
| *PCM-TD-PBE0/6-311G(d,p)* | | | | |
| M06-HF/6-31G(d) geometry | | | | |
| $S_0 \rightarrow S_1$ | 425 | 2.92 | 1.231 | H → L (90 %) |
| $S_0 \rightarrow S_2$ | 366 | 3.39 | 0.057 | H-1 → L (91 %) |
| $S_0 \rightarrow S_3$ | 353 | 3.51 | 0.084 | H-2 → L (88 %) |
| $S_0 \rightarrow S_4$ | 338 | 3.67 | 0.127 | H → L + 1 (86 %) |
| M06-2X/6-31G(d) geometry | | | | |
| $S_0 \rightarrow S_1$ | 460 | 2.70 | 1.640 | H → L (97 %) |
| $S_0 \rightarrow S_2$ | 376 | 3.30 | 0.039 | H-1 → L (93 %) |
| $S_0 \rightarrow S_3$ | 362 | 3.43 | 0.030 | H-2 → L (93 %) |
| $S_0 \rightarrow S_4$ | 343 | 3.61 | 0.062 | H → L + 1 (94 %) |
| MP2/6-31G(d) geometry | | | | |
| $S_0 \rightarrow S_1$ | 439 | 2.82 | 1.412 | H → L (87 %) |
| $S_0 \rightarrow S_2$ | 365 | 3.40 | 0.012 | H-1 → L (87 %) |
| $S_0 \rightarrow S_3$ | 340 | 3.65 | 0.252 | H → L + 1 (78 %) |
| $S_0 \rightarrow S_4$ | 336 | 3.69 | 0.108 | H-2 → L (78 %) |
| *PCM-TD-CAM-B3LYP/6-311G(d,p)* | | | | |
| M06-HF/6-31G(d) geometry | | | | |
| $S_0 \rightarrow S_1$ | 362 | 3.42 | 1.703 | H → L (74 %) |
| $S_0 \rightarrow S_2$ | 315 | 3.93 | 0.009 | H-2 → L (46 %) + H-1 → L (20 %) |
| $S_0 \rightarrow S_3$ | 298 | 4.16 | 0.095 | H-2 → L (26 %) + H-1 → L (23 %) |
| $S_0 \rightarrow S_4$ | 277 | 4.47 | 0.145 | H-3 → L (36 %) + H → L + 1 (17 %) |
| M06-2X/6-31G(d) geometry | | | | |
| $S_0 \rightarrow S_1$ | 406 | 3.05 | 1.917 | H → L (84 %) |
| $S_0 \rightarrow S_2$ | 330 | 3.76 | 0.028 | H-2 → L (−30 %) + H-1 → L (37 %) |
| $S_0 \rightarrow S_3$ | 312 | 3.97 | 0.075 | H-2 → L (44 %) + H-1 → L (17 %) |
| $S_0 \rightarrow S_4$ | 292 | 4.24 | 0.117 | H-3 → L (43 %) + H → L + 1 (19 %) |
| MP2/6-31G(d) geometry | | | | |
| $S_0 \rightarrow S_1$ | 382 | 3.25 | 1.754 | H → L (78 %) |
| $S_0 \rightarrow S_2$ | 310 | 4.00 | 0.005 | H-2 → L (−12 %) + H-1 → L (35 %) |
| $S_0 \rightarrow S_3$ | 302 | 4.11 | 0.147 | H-2 → L (58 %) + H-1 → L (10 %) |
| $S_0 \rightarrow S_4$ | 281 | 4.41 | 0.076 | H-3 → L (28 %) + H-4 → L (−27 %) |
| Expt. | 430 | 2.88 | | |

system. The CAM-B3LYP was also examined for taking account of the long-range corrections for describing this system. The CAM-(Coulomb-attenuating method) B3LYP was also examined for taking account of the long-range corrections for describing the long $\pi$-conjugation. The wavelength of the structures obtained from M06-2X method 406 (3.05 eV) is closer to experimental data of 430 nm (2.88 eV) than from M06-HF and MP2 methods. This indicates that the Minnesota classes of M06-2X functionals with long-range and/or dispersion corrections hybrids or double-hybrids are more accurate than the M06-HF and MP2 levels of theory [50, 61–65]. From our calculated electronic transitions with PCM-TD-CAM-B3LYP method compared with the experimental data, the results from the ground-state geometries of $OPV_3$–COOH derivatives using M06-2X/6-31G(d) optimization are in better agreement than obtained from M06-HF and MP2 methods. M06-HF is not as good as other high-quality density functionals for valence excitations. It is the best for long-range charge-transfer excitation. When the use of full Hartree–Fock exchange is important, for example to avoid the error of self-interaction at long-range, the M06-HF functional can be recommended since it has reasonably good overall performance (excluding transition metals), even though it has full Hartree–Fock exchange [41, 42].

The TD-CAM-B3LYP excitation spectra for these optimized structures are compared to the experimental absorption spectra in Fig. 3. The maximum absorption region of $OPV_3$–COOH is the excitation from HOMO to LUMO at 430 nm. The experimental spectra were observed in toluene and consist of two absorption bands at 430 and $\sim$325 nm. The TD-CAM-B3LYP absorption spectrum of the compound shows two distinct absorption bands, which is in good agreement with the experimental spectra. Based on M06-2X, geometry has two peaks with a large oscillator strength, whereas the spectra of MP2 and M06-HF geometries show underestimation. These trends were well reproduced by the present TD-CAM-B3LYP calculations based on M06-2X optimization geometry. The M06-2X/6-31G(d) method is therefore selected for the ground-state geometry optimization. The non-planar geometries were selected to study the effect of spacer and anchor (or acceptor) groups of $OPV_3$–COOH molecule.

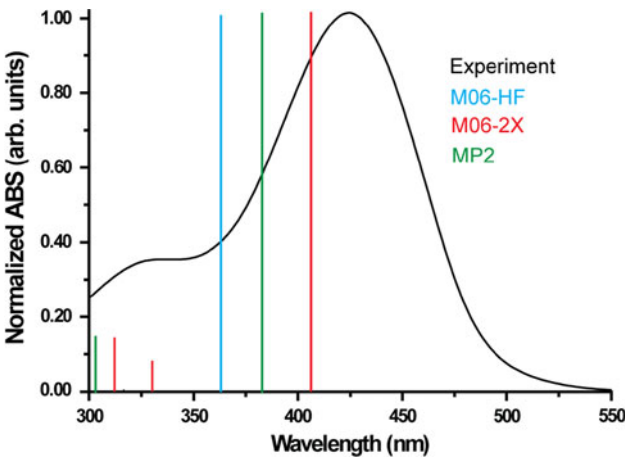


**Fig. 3** Comparison of experimental spectrum (*black line*) and simulated absorption spectra with combined PCM-TD-CAM-B3LYP/6-311G(d,p) method and PCM solvent effect of toluene from M06-HF (*blue line*), M06-2X (*red line*) and MP2 (*green line*) optimized ground-state geometry

The molecular orbitals of $OPV_3$–COOH of the electronic transition states were calculated with PCM-TD-CAM-B3LYP/6-311G(d,p). The molecular orbitals are depicted in Fig. 4. The $S_0 \rightarrow S_1$ transition has the larger oscillator strength as the most probable transition from ground state to excited state of all transitions, corresponding to excitation from HOMO to LUMO. The LUMO orbital possesses a larger contribution of the carboxyl group, which is called anchor or acceptor group, located at the end of phenylene ring compared with the HOMO orbital, which is mainly located at the three phenylene rings. The electronic transition of $OPV_3$–COOH indicates that when an electron at ground state is excited by a photon from the sunlight, electron would transfer from the $OPV_3$–COOH to $TiO_2$ electrode. Because $OPV_3$–COOH is anchored onto the $TiO_2$ surface through carboxylic acid, electron injection process will be facilitated as the molecule is excited. The photoinduced electron transfer across the dye-semiconductor interface is governed by the electronic properties of the interface.

### 3.2 Effect of spacer groups and anchor

Into the non-planar ground-state geometry of $OPV_3$–COOH, various thiophene spacer groups were inserted, in particular one thiophene subunit, dithiophene and vinylene-thiophene (Fig. 1). These spacer groups are used for the synthesis of compounds that are expected to possess broad absorption spectra in the visible light region, an intense absorption and an increase in the electron transfer to the semiconductor. Additionally, a cyanoacrylic substituent with a strong electron withdrawing group as anchor leads to a new compound, which is used for a detailed investigation. The ground-state geometries were optimized using M06-2X/6-31G(d) level of theory, and the electronic transitions were calculated using PCM-TD-CAM-B3LYP/6-311G(d,p) level of calculation. First, the ground-state geometries are studied. The structures are shown in Table 3. The ground-state geometries of $OPV_3$–CNCOOH, $OPV_3$–Th–CNCOOH, OPV3–diTh–CNCOOH and $OPV_3$–viTh–CNCOOH and particularly the torsion angles are similar compared with $OPV_3$–COOH. The conformations of these structures are non-planar as the phenylene rings

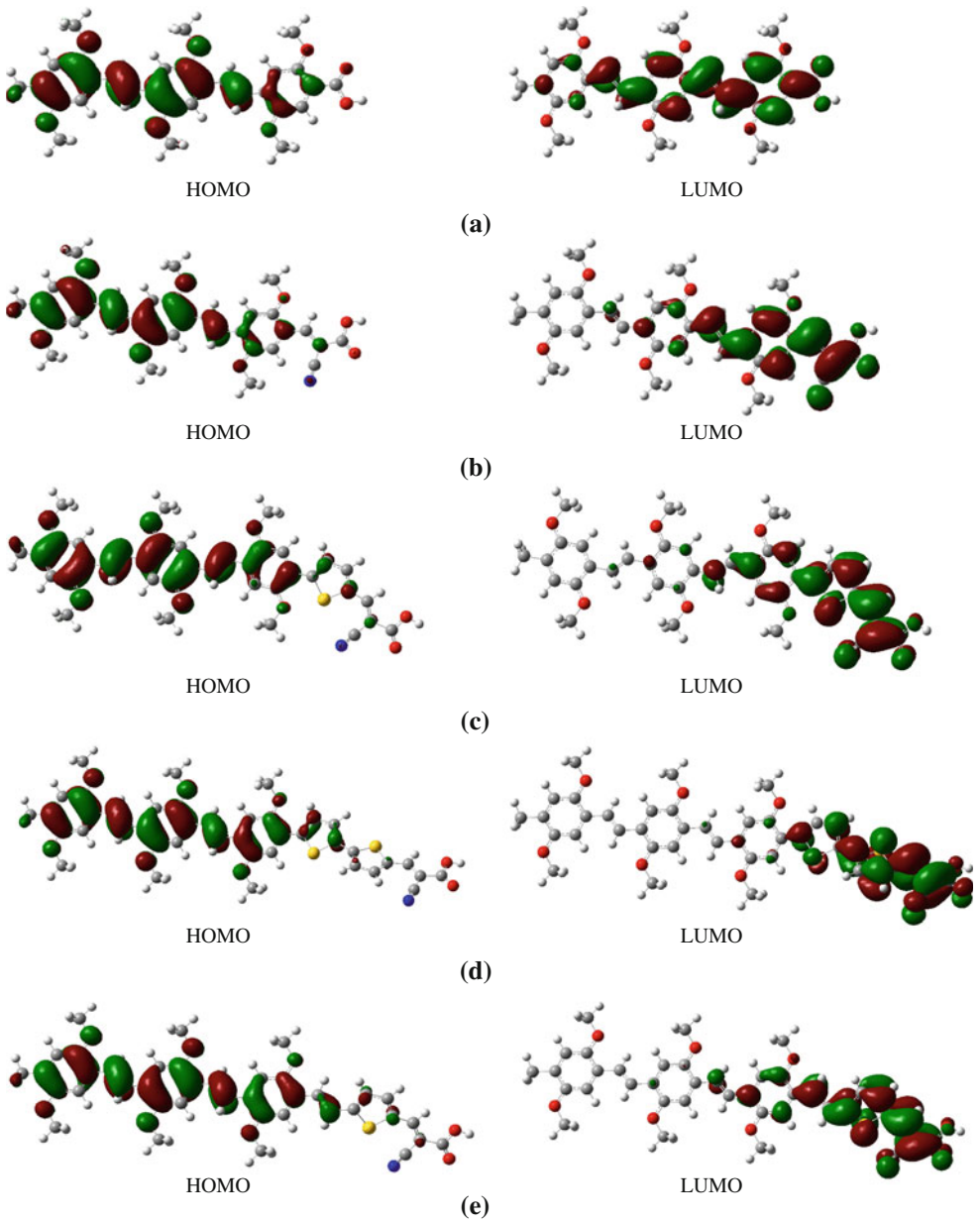


**Fig. 4** Plots of the CAM-B3LYP/6-311G(d,p) molecular orbitals contributing significantly to the lowest energy transitions of studied molecules for (**a**) $OPV_3$–COOH, (**b**) $OPV_3$–CNCOOH, (**c**) $OPV_3$–Th–CNCOOH, (**d**) $OPV_3$–diTh–CNCOOH and (**e**) $OPV_3$–viTh–CNCOOH. Depicted are two isosurfaces of equal values but opposite sign

are not in the plane of the linkers. The geometry optimization results show that the conformation of the chromophore for all compounds is non-planar, but the conformation of the spacer linkage twists out of the plane of the chromophore. In previous work, we showed the electronic properties of each conformers of DMTB in the three isomers, EE-, EZ- and ZZ- isomers [66]. It is indicated that depending on the conformation of the spacer linkage in the system can have a decisive influence on the shape of a spectrum. Therefore, these structures were confirmed to be global minimum by the vibrational frequency analysis. The torsion angles between chromophore and thiophene linkages in $OPV_3$–Th–CNCOOH (38°) are more twisted than that of the vinylene linkage in $OPV_3$–viTh–CNCOOH (25°).

The most probable transitions of all compounds, which account from the highest oscillator strength, are listed in Table 4. The oscillator strength of $OPV_3$–COOH, $OPV_3$–CNCOOH, $OPV_3$–Th–CNCOOH, OPV3–diTh–CNCOOH and $OPV_3$–viTh–CNCOOH is 1.917, 2.096, 2.325, 2.831 and 2.835, respectively, corresponding to $S_0 \rightarrow S_1$ (HOMO → LUMO) transition at 406, 460, 456, 466 and

**Table 3** Structural parameters of $OPV_3$–CNCOOH derivatives obtained from fully optimization by M06-2X functional at 6-31G(d) level of basis set (bond lengths in Ångstrom, angles in degrees)

| Parameters | $OPV_3$–COOH | $OPV_3$–CNCOOH | $OPV_3$–Th–CNCOOH | $OPV_3$–diTh–CNCOOH | $OPV_3$–viTh–CNCOOH |
|---|---|---|---|---|---|
| Bond length | | | | | |
| C1–C2 | 1.398 | 1.389 | 1.398 | 1.398 | 1.398 |
| C2–C3 | 1.388 | 1.394 | 1.388 | 1.388 | 1.388 |
| C3–C4 | 1.407 | 1.404 | 1.407 | 1.408 | 1.408 |
| C4–C5 | 1.399 | 1.401 | 1.399 | 1.399 | 1.399 |
| C5–C6 | 1.387 | 1.386 | 1.387 | 1.386 | 1.386 |
| C6–C1 | 1.408 | 1.402 | 1.408 | 1.408 | 1.409 |
| C4–C7 | 1.463 | 1.465 | 1.463 | 1.463 | 1.462 |
| C7–C8 | 1.342 | 1.342 | 1.342 | 1.342 | 1.343 |
| C8–C9 | 1.465 | 1.464 | 1.463 | 1.464 | 1.463 |
| Bond angle | | | | | |
| C3–C4–C7 | 119.6 | 119.6 | 119.6 | 119.4 | 119.5 |
| C4–C7–C8 | 125.8 | 125.9 | 125.9 | 126.2 | 126.2 |
| Torsion angle | | | | | |
| C5–C4–C7–C8 | −15.7 | −10.4 | −16.0 | −9.6 | −7.8 |
| C7–C8–C9–C10 | 18.6 | 15.0 | 18.8 | 11.6 | 9.0 |
| H-bond | | | | | |
| R1(O–H) | 2.329 | 2.329 | 2.330 | 2.335 | 2.304 |
| R2(O–H) | 2.330 | 2.337 | 2.335 | 2.333 | 2.307 |
| R3(O–H) | 2.322 | 2.298 | 2.326 | 2.295 | 2.292 |
| R4(O–H) | 2.332 | 2.308 | 2.345 | 2.311 | 2.292 |
| BLA | 0.260 | 0.182 | 0.209 | 0.180 | 0.178 |

BLA and the mean relative error values are also listed

490 nm, respectively, whereas, the second absorption regions are 292, 302, 321, 339 and 334 nm, respectively. The calculated absorption spectra of all compounds including the toluene solvation effect are simulated and presented in Fig. 5. From $OPV_3$–COOH, $OPV_3$–CNCOOH, $OPV_3$–Th–CNCOOH, $OPV_3$–diTh–CNCOOH and $OPV_3$–viTh–CNCOOH, the conjugated structures become more extended, although their phenylenevinylene chromophores are the same. The maximum absorption spectra of all compounds are red-shifted to 406, 460, 456, 466 and 490 nm with the expansion of their conjugated systems. The red-shift to the visible range in the absorption spectra of the $\pi$-conjugated system from $OPV_3$–COOH, $OPV_3$–CNCOOH, $OPV_3$–Th–CNCOOH, $OPV_3$–diTh–CNCOOH and $OPV_3$–viTh–CNCOOH is desirable for absorbing the sunlight and good employing as photo-sensitizer in DSSCs. Comparing different types of functional spacers, the absorption wavelength of $OPV_3$–viTh–CNCOOH (490 and 334 nm) and $OPV_3$–diTh–CNCOOH (466 and 339 nm) is longer than that of $OPV_3$–Th–CNCOOH (456 and 321 nm) because $OPV_3$–viTh–CNCOOH is more planar than $OPV_3$–Th–CNCOOH, as a consequence of the more extended $\pi$-conjugated system. The absorption wavelength of $OPV_3$–viTh–CNCOOH and $OPV_3$–diTh–CNCOOH is more red-shifted than that of $OPV_3$–Th–CNCOOH, which is in agreement with results found for other function spacers [6, 9, 10, 18]. Then, vinylene linkage spacers lead to a more planar conformation, high $\pi$-conjugation and broad absorption in visible region compared with the thiophene linkage. Therefore, the introduction of different spacer group (thiophene, dithiophene and vinylenethiophene) has a substantial influence on the resultant electronic properties of $OPV_3$–diTh–CNCOOH derivatives.

The HOMO and LUMO orbitals of all compounds are shown in Fig. 4. The LUMO orbital possesses for all compounds contributions to the carboxyl group, and a larger contribution of the thiophene spacer group near the carboxyl groups is observed. The results show that electron transfer from phenylenevinylene chromophore via thiophene spacer to carboxyl anchor group takes place during the excitation process of $OPV_3$–CNCOOH, $OPV_3$–Th–CNCOOH, $OPV_3$–diTh–CNCOOH and $OPV_3$–viTh–CNCOOH. The percentages of electron polarization that expands the different density of molecular orbitals between HOMO and LUMO of all compounds were calculated to explain the electron transfer from ground state to excited state. These results are shown in Table 5. The structures

**Table 4** Calculated electronic transitions for $OPV_3$–COOH, $OPV_3$–CNCOOH, $OPV_3$–Th–CNCOOH, $OPV_3$–diTh–CNCOOH and $OPV_3$–viTh–CNCOOH using PCM-TD-CAM-B3LYP/6-311G(d,p)//M06-2X/6-31G(d) in toluene solvent

| State | nm | eV | *f* | Transition characters |
|---|---|---|---|---|
| $OPV_3$–COOH | | | | |
| $S_0 \rightarrow S_1$ | 406 | 3.05 | 1.917 | H → L (84 %) |
| $S_0 \rightarrow S_2$ | 330 | 3.76 | 0.028 | H-2 → L (−30 %) + H-1 → L (37 %) |
| $S_0 \rightarrow S_3$ | 312 | 3.97 | 0.075 | H-2 → L (44 %) + H-1 → L (17 %) |
| $S_0 \rightarrow S_4$ | 292 | 4.24 | 0.117 | H-3 → L (43 %) + H → L + 1 (19 %) |
| $S_0 \rightarrow S_5$ | 278 | 4.46 | 0.074 | H → L + 1 (33 %) + H-3 → L (−20 %) |
| $OPV_3$–CNCOOH | | | | |
| $S_0 \rightarrow S_1$ | 460 | 2.69 | 2.096 | H → L (68 %) + H-1 → L (16 %) |
| $S_0 \rightarrow S_2$ | 372 | 3.33 | 0.084 | H-2 → L (44 %) + H-1 → L (−20 %) |
| $S_0 \rightarrow S_3$ | 329 | 3.77 | 0.089 | H → L + 1 (36 %) + H-2 → L (−18 %) |
| $S_0 \rightarrow S_4$ | 318 | 3.90 | 0.075 | H-3 → L (20 %) + H-4 → L (−13 %) |
| $S_0 \rightarrow S_5$ | 302 | 4.10 | 0.292 | H-4 → L (22 %) + H → L + 1 (18 %) |
| $OPV_3$–Th–CNCOOH | | | | |
| $S_0 \rightarrow S_1$ | 456 | 2.72 | 2.325 | H → L (53 %) + H-1 → L (−21 %) |
| $S_0 \rightarrow S_2$ | 376 | 3.30 | 0.217 | H → L + 1 (50 %) + H-1 → L (21 %) |
| $S_0 \rightarrow S_3$ | 326 | 3.80 | 0.007 | H-4 → L (35 %) + H → L (−14 %) |
| $S_0 \rightarrow S_4$ | 321 | 3.86 | 0.400 | H-4 → L (32 %) + H → L + 1 (20 %) |
| $S_0 \rightarrow S_5$ | 313 | 3.96 | 0.008 | H-2 → L + 1 (−20 %) + H-1 → L + 1 (25 %) |
| $OPV_3$–diTh–CNCOOH | | | | |
| $S_0 \rightarrow S_1$ | 466 | 2.66 | 2.831 | H → L (39 %) + H-1 → L (−25 %) |
| $S_0 \rightarrow S_2$ | 396 | 3.13 | 0.286 | H → L + 1(54 %) + H-1 → L (14 %) |
| $S_0 \rightarrow S_3$ | 339 | 3.66 | 0.322 | H-3 → L (34 %) + H-1 → L + 1 (16 %) |
| $S_0 \rightarrow S_4$ | 332 | 3.73 | 0.056 | H → L (39 %) + H-1 → L + 1 (25 %) |
| $S_0 \rightarrow S_5$ | 312 | 3.97 | 0.047 | H-2 → L + 1 (35 %) |
| $OPV_3$–viTh–CNCOOH | | | | |
| $S_0 \rightarrow S_1$ | 490 | 2.53 | 2.835 | H → L (55 %) + H-1 → L (−21 %) |
| $S_0 \rightarrow S_2$ | 391 | 3.17 | 0.185 | H → L + 1 (48 %) + H-1 → L (−23 %) |
| $S_0 \rightarrow S_3$ | 340 | 3.64 | 0.091 | H-3 → L (48 %) + H-1 → L + 1 (20 %) |
| $S_0 \rightarrow S_4$ | 334 | 3.72 | 0.323 | H → L (34 %) + H → L + 1 (18 %) |
| $S_0 \rightarrow S_5$ | 318 | 3.90 | 0.027 | H-2 → L + 1 (22 %) + H-1 → L + 1 (17 %) |

were separated into 4 parts, OPV1, OPV2, spacer and anchor. The difference of percent distribution between HOMO and LUMO for $OPV_3$–COOH at anchor part is very small (9 %), compared with $OPV_3$–CNCOOH (50 %), $OPV_3$–Th–CNCOOH (47 %), $OPV_3$–diTh–CNCOOH (52 %) and $OPV_3$–viTh–CNCOOH (45 %), which increases to ~80 % at OPV1, but decreases at OPV2, part for $OPV_3$–CNCOOH derivatives. The results indicate that electrons at chromophores (OPV1 and OPV2 parts) transfer to the anchor during excitation from HOMO to LUMO in the case of $OPV_3$–COOH and delocalize via spacer toward anchor in $OPV_3$–Th–CNCOOH derivatives. Then, the anchor (acceptor) group in $OPV_3$–COOH and $OPV_3$–CNCOOH derivatives that interacts with the surface of $TiO_2$ causes electron transfer from phenylenevinylene (chromophore) to anchor groups and injects electrons to the conduction band of $TiO_2$. Moreover, spacer groups that link between chromophore and acceptor such as thiophene and vinylenethiophene increase the electron transfer value from chromophore to anchor group in $OPV_3$–CNCOOH derivatives.

The molecular orbitals (Fig. 4) and the percentage of electron polarization (Table 5) demonstrate that $OPV_3$–CNCOOH derivatives can increase the efficiency of electron transfer from 9 % in carboxyl group of $OPV_3$–COOH to 50 % in acrylic group. Then, the electron injection process from acrylic anchor group to the semiconductor conduction band is more probable than that of the carboxyl group. Additionally, the effects of spacer groups for increase in the efficiency of electron transfer were considered. Although the absorption wavelength of the vinylene linkage is longer than that of thiophene linkage, the

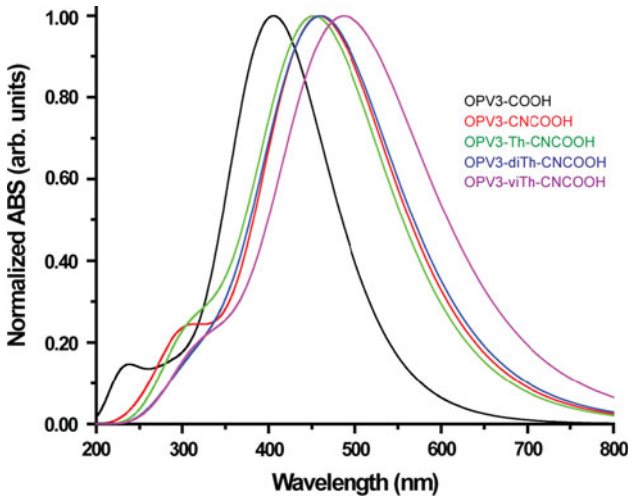


**Fig. 5** Comparison of simulated absorption spectra for $OPV_3$–COOH, $OPV_3$–CNCOOH, $OPV_3$–Th–CNCOOH, $OPV_3$–diTh–CNCOOH and $OPV_3$–viTh–CNCOOH using PCM-TD-CAM-B3LYP/6-311G(d,p) method

percentage of electron transfer at spacer and anchor groups of $OPV_3$–viTh–CNCOOH (83 %), $OPV_3$–Th–CNCOOH (77 %) and $OPV_3$–diTh–CNCOOH (77 %) is higher than of $OPV_3$–CNCOOH (50 %) and $OPV_3$–COOH (9 %). It indicates that the thiophene linkage spacer can increase the efficiency of electron transfer from chromophore to anchor more than the vinylene linkage spacer. However, the limit of cyanoacrylic acid group is about 50 % to receive electrons from chromophore and spacer.

As discussed about efficient charge injection, this is an important parameter for a sensitizer in DSSCs. The ionization potential (IP) and electron affinity (EA) are used to evaluate the energy barrier for injection of holes and electrons. The calculated results at M06-2X/6-31G(d) are listed in Table 6. The $OPV_3$–CNCOOH derivatives have a lower IP, −6.76 eV ($OPV_3$–CNCOOH), −6.67 eV ($OPV_3$–Th–CNCOOH), −6.63 eV ($OPV_3$–diTh–CNCOOH), −6.63 eV ($OPV_3$–viTh–CNCOOH) and a higher EA, −1.40 eV ($OPV_3$–CNCOOH), −1.35 eV ($OPV_3$–Th–CNCOOH), −1.53 eV ($OPV_3$–diTh–CNCOOH), −1.53 eV ($OPV_3$–viTh–CNCOOH) values compared to $OPV_3$–COOH, −6.71 eV (IP) and −0.71 eV (EA). The lower IP value (in the range of −6.63 to −6.76 eV) of $OPV_3$–CNCOOH derivatives indicates that the entrance of holes from the conducting transparent oxide to the hole-transport layer is easier compared to $OPV_3$–COOH. The same analogy was found for the higher EA value of $OPV_3$–CNCOOH derivatives, where there was an easier entrance of electrons from cathode to the electron-transport layer [3, 67]. This indicates that the use of spacer and cyanoacrylic groups resulted in the increase in the creation of holes and electrons.

The charge mobility in organic materials can be described as a sequence of uncorrelated hops. In the case of self-exchange reactions, i.e., electron-transfer reaction from a charged species to an adjacent neutral unit, the rate of charge transfer can be approximately described. The reorganization energy [68–70] is the energy required for all structural adjustments, which are needed in order to adopt the configuration of the compound that is necessary for the electron transfer process. The reorganization energy is mainly influenced by $\lambda_i$, which can be calculated according to the following formula

$$\lambda_i = \left[E_0^{\pm} - E_{\pm}^{\pm}\right] + \left[E_{\pm} - E_0\right] \quad (3)$$

where $E_0^{\pm}$ is the energy of the cation (anion) calculated with the optimized structure of the neutral molecule, $E_{\pm}^{\pm}$ is the energy of the cation (anion) calculated with the optimized cation (anion) structure, $E_{\pm}$ is the energy of the neutral molecule calculated at the cationic (anionic) state and $E_0$ is the energy of the neutral molecule at ground state.

Table 6 lists the calculated internal reorganization energies for both holes ($\lambda_{\text{Hole}}$) and electrons ($\lambda_{\text{Electron}}$) calculated at M06-2X/6-31G(d). We then compared the reorganization energies with the short-circuit current density ($J_{sc}$), since $J_{sc}$ values depend on the generation and collection of light generated carriers. It was observed that the trend for the total reorganization energies ($\lambda_{\text{Total}}$) was inversely proportional to the $J_{sc}$, i.e. as $\lambda_{\text{Total}}$ decreases, the $J_{sc}$ value increases, which was consistent with Eq. (3) that minimizing $\lambda$ leads to a high electron-transfer rate [71]. Furthermore, the magnitudes of the charge-carrier transport rates should be balanced in order to attain a high luminous efficiency. The total reorganization energies for $OPV_3$–CNCOOH derivatives are lower, 1.66 eV ($OPV_3$–CNCOOH), 1.58 eV ($OPV_3$–Th–CNCOOH), 1.56 eV ($OPV_3$–diTh–CNCOOH) and 1.66 eV ($OPV_3$–viTh–CNCOOH) than the energy of $OPV_3$–COOH (1.84 eV). Upon comparison of the rates of the charge-carrier transport for both of the analogues, $OPV_3$–CNCOOH derivatives result in a more balanced transport rates than $OPV_3$–COOH due to the addition of spacer and cyanoacrylic group to $OPV_3$–COOH increasing the probability of confined excitons in the emitting layer as observed in other DSSCs [72, 73]. These data are confirmed by the results of previous studies [74–76]. Hagberg and coworker [17] had synthesized a series of organic chromophores in order to approach optimal energy level composition in the $TiO_2$-dye-iodide/triiodide system in the DSSCs. They found that HOMO and LUMO energy level tuning is achieved by varying the conjugation between the triphenylamine donor and the cyanoacetic acid acceptor. The percentage efficiencies (%$\eta$) of vinylenethiophen (–viTh–CNCOOH) chromophores (%$\eta$ = 3.08) show more satisfactory efficiencies than –diTh–CNCOOH (%$\eta$ = 2.75), –Th–CNCOOH (%$\eta$ = 2.75) and –CNCOOH chromophores (%$\eta$ = 1.55) on thin

**Table 5** The percentage of electron polarizations of HOMO and LUMO for $OPV_3$–COOH, $OPV_3$–CNCOOH, $OPV_3$–Th–CNCOOH, $OPV_3$–diTh–CNCOOH, and $OPV_3$–viTh–CNCOOH

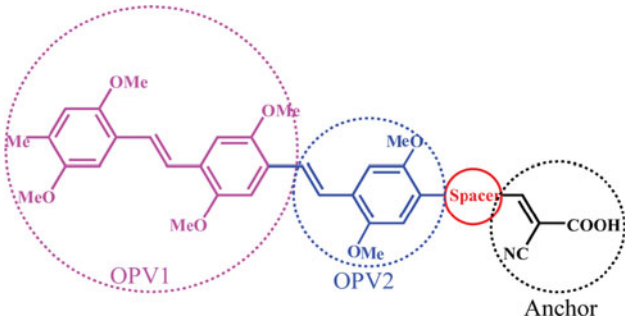


| Compounds | State | % Electron polarizations | | | |
|---|---|---|---|---|---|
| | | OPV1 | OPV2 | Spacer | Anchor |
| $OPV_3$–COOH | | | | | |
| | LUMO + 1 | 66 | 24 | – | 10 |
| | LUMO | 57 | 34 | – | 10 |
| | HOMO | 92 | 7 | – | 1 |
| | HOMO − 1 | 81 | 18 | – | 1 |
| | Δ%H → L | 35 | −27 | – | −9 |
| $OPV_3$–CNCOOH | | | | | |
| | LUMO + 1 | 83 | 5 | – | 12 |
| | LUMO | 16 | 32 | – | 52 |
| | HOMO | 92 | 6 | – | 2 |
| | HOMO − 1 | 84 | 13 | – | 3 |
| | Δ%H → L | 76 | −26 | – | −50 |
| $OPV_3$–Th–CNCOOH | | | | | |
| | LUMO + 1 | 73 | 13 | 5 | 9 |
| | LUMO | 6 | 13 | 33 | 48 |
| | HOMO | 86 | 10 | 3 | 1 |
| | HOMO − 1 | 77 | 23 | 7 | 3 |
| | Δ%H → L | 80 | −3 | −30 | −47 |
| $OPV_3$–diTh–CNCOOH | | | | | |
| | LUMO + 1 | 41 | 25 | 18 | 6 |
| | LUMO | 1 | 3 | 44 | 52 |
| | HOMO | 82 | 13 | 5 | 0 |
| | HOMO − 1 | 57 | 28 | 14 | 1 |
| | Δ%H → L | 81 | 10 | −39 | −52 |
| $OPV_3$–viTh–CNCOOH | | | | | |
| | LUMO + 1 | 51 | 22 | 15 | 12 |
| | LUMO | 3 | 8 | 43 | 46 |
| | HOMO | 81 | 14 | 5 | 1 |
| | HOMO − 1 | 57 | 29 | 11 | 2 |
| | Δ%H → L | 78 | 6 | −38 | −45 |

$TiO_2$ films. These results show that tuning of the chromophores was successful and fulfilled the thermodynamic criteria for DSSCs. Thus, the theoretical studies of the electronic properties are important to design the superior organic dye molecules.

## 4 Conclusions

The optimized structural parameters of $OPV_3$–COOH and $OPV_3$–CNCOOH derivatives obtained from hybrid functional M06-HF, M06-2X and MP2 method at

**Table 6** Ionization potential (IP), electron affinity (EA), intramolecular reorganization energies for hole ($\lambda_{Hole}$) and electron ($\lambda_{Electron}$) transport calculated by M06-2X/6-31G(d)

| Parameter | $OPV_3$–COOH | $OPV_3$–CNCOOH | $OPV_3$–Th–CNCOOH | $OPV_3$–diTh–CNCOOH | $OPV_3$–viTh–CNCOOH |
|---|---|---|---|---|---|
| IP (eV) | −6.71 | −6.76 | −6.67 | −6.66 | −6.63 |
| EA (eV) | −0.71 | −1.40 | −1.35 | −1.51 | −1.53 |
| $\lambda_{Hole}$ (eV) | 0.85 | 0.89 | 0.87 | 0.86 | 0.87 |
| $\lambda_{Electron}$ (eV) | 0.99 | 0.77 | 0.71 | 0.69 | 0.79 |
| $\lambda_{Total}$ (eV) | 1.84 | 1.66 | 1.58 | 1.56 | 1.66 |

6-31G(d) level are in agreement with the experimental data. The results show that in these structures, weak intramolecular hydrogen bonding occurs between the oxygen atoms of substituted alkoxy groups and the phenylene ring at the ortho-carbon and the hydrogen atom at the vinylene linkage. However, the systems are non-planar in the ground state. The structures of $OPV_3$–COOH obtained from various methods were used to calculate the electronic transitions using TD-CAM-B3LYP/6-311G(d,p) including CPCM toluene solvation effect to compare with the absorption band of this molecule in toluene. The result of the non-planar structure using M06-2X/6-31G(d) is closer to the experimental absorption data than the more planar structure using B3LYP/6-31G(d). The MP2/6-31G(d) calculations confirm the results of M06-2X/6-31G(d) very well. Therefore, in this study, PCM-TD-CAM-B3LYP/6-311G(d,p)//M06-2X/6-31G(d) and the non-planar ground-state geometry of phenylenevinylene chromophore were selected to investigate the effects of spacer and anchor groups for the structures and electronic properties of $OPV_3$–CNCOOH derivatives.

The anchor or acceptor group such as carboxylic acid that interacts with the surface of the semiconductor causes electron transfer from the chromophore to this anchor group. The spacer group such as thiophene that links between chromophore and anchor group increases the electron transfer and expands the $\pi$-conjugated system to cause absorption bands in the visible light region. The enhanced electron transfer and the red-shift in the absorption band from $OPV_3$–COOH, $OPV_3$–CNCOOH to $OPV_3$–Th–CNCOOH, $OPV_3$–diTh–CNCOOH and $OPV_3$–viTh–CNCOOH are desirable for gaining the sunlight and good employing as photo-sensitizer in DSSCs. The molecular orbitals and HOMO–LUMO energy values for $OPV_3$–CNCOOH derivatives demonstrate that the electron will transfer from the phenylenevinylene chromophore toward the spacer groups and inject to the carboxyl anchor group during the excitation process. Therefore, $OPV_3$–CNCOOH derivatives can be used for sensitizer in DSSCs. The modeling of spacer and anchor groups in this study may suggest new sensitizer compound that enhances the efficiency of electron transfer and absorption of sunlight for the synthesis of new materials.

**Acknowledgments** Support from the Thailand Research Fund (RTA5380010 to SH and MRG5480273 to SS). SS was supported from the Asea-Uninet, the University of Vienna and Science Research Fund (ScRF), and ScAWAKE from Faculty of Science, Kasetsart University. Center of Nanotechnology Kasetsart University, Kasetsart University Research and Development Institute (KURDI), National Nanotechnology Center (NANOTEC), Laboratory of Computational and Applied Chemistry (LCAC), the Commission on Higher Education, Ministry of Education [trough "the National Research University Project of Thailand (NRU)" and the "National Center of Excellence for Petroleum, Petrochemical and Advanced Materials (NCEPPAM)"] are gratefully acknowledged for research facilities. The calculations were performed in part on the Schrödinger III cluster and the VSC of the University of Vienna.

## References

1. Günes S, Sariciftci NS (2008) Hybrid solar cells. Inorg Chim Acta 361(3):581–588
2. Grätzel M (2009) Recent advances in sensitized mesoscopic solar cells. Acc Chem Res 42(11):1788–1798
3. Regan BO, Grätzel M (1991) A low-cost, high-efficiency solar cell based on dye-sensitized colloidal $TiO_2$ films. Nature 353(6346):737–740
4. Goncalves LM, Bermudez VZ, Ribeiro HA, Mendes AM (2008) Dye-sensitized solar cells: A safe bet for the future. Energy Environ Sci 1(6):655–680
5. Nazeeruddin MK, Kay A, Rodicio L, Humphry-Baker R, Müller E, Liska P, Vlachopoulos N, Grätzel M (1993) Conversion of light to electricity by cis-$X_2$bis(2,2′-bipyridyl-4,4′-dicarboxylate)ruthenium(II) charge-transfer sensitizers (X = Cl-, Br-, I-, CN-, and SCN-) on nanocrystalline titanium dioxide electrodes. J. J Am Chem Soc 115(14):6382–6390
6. Mishra A, Fischer MKR, Büerle P (2009) Enhancement of electrogenerated chemilumines-cence and radical stability by peripheral multidonors on alkynylpyrene derivatives. Angew Chem Int Ed 48(14):2474–2499
7. Ito S, Zakeeruddin M, Hummphrey-Baker R, Liska P, Charvet R, Comte P, Nazeeruddin MK, Pechy P, Takata M, Miura H, Uchida S, Grätzel M (2006) High-efficiency organic-dye-sensitized solar cells controlled by nanocrystalline-$TiO_2$ electrode thickness. Adv Mater 18(9):1202–1205
8. Ito S, Miura H, Uchida S, Takata M, Sumioka K, Liska P, Comte P, Pechy P, Grätzel M (2008) High-conversion-efficiency organic dye-sensitized solar cells with a novel indoline dye. Chem Commun 41:5194–5196

9. Choi H, Baik C, Kang SO, Ko J, Kang M-S, Nazeeruddin MK, Grätzel M (2008) Highly efficient and thermally stable organic sensitizers for solvent-free dye-sensitized solar cells. Angew Chem Int Ed 47(2):327–330
10. Zhang G, Bala H, Cheng Y, Shi D, Lv X, Yu Q, Wang P (2009) High efficiency and stable dye-sensitized solar cells with an organic chromophore featuring a binary π-conjugated spacer. Chem Commun 16:2198–2200
11. Van Hal PA, Wienk MM, Kroon JM, Janssen RAJ (2003) $TiO_2$ sensitized with an oligo(*p*-phenylenevinylene) carboxylic acid: a new model compound for a hybrid solar cell. J Mater Chem 13(5):1054–1057
12. Kim C, Choi H, Kim S, Baik C, Song K, Kang M-S, Kang SO, Ko J (2008) Molecular engineering of organic sensitizers containing *p*-phenylene vinylene unit for dye-sensitized solar cells. J Org Chem 73(18):7072–7079
13. Jang S-R, Lee C, Choi H, Ko JJ, Lee J, Vittal R, Kim K-J (2006) Oligophenylenevinylene-functionalized Ru(II)-bipyridine sensitizers for efficient dye-sensitized nanocrystalline $TiO_2$ solar cells. Chem Mater 18(23):5604–5608
14. Li S-L, Jiang K-J, Shao K-F, Yang L-M (2006) Novel organic dyes for efficient dye-sensitized solar cells. Chem Commun 26:2792–2794
15. Suramitr S, Hannongbua S, Wolschann P (2007) Conformational analysis and electronic transition of carbazole-based oligomers as explained by density functional theory. J Mol Struct (THEOCHEM) 807(1–3):109–119
16. Meeto W, Suramitr S, Vannarat S, Hannongbua S (2008) Structural and electronic properties of poly(fluorene-vinylene) copolymer and its derivatives: Time-dependent density functional theory investigation. Chem Phys 349(1–3):1–8
17. Hagberg DP, Edvinsson T, Marinado T, Boschloo G, Hagfeldt A, Sun L (2006) A novel organic chromophore for dye-sensitized nanostructured solar cells. Chem Commun 21:2245–2247
18. Chen R, Yang X, Tian H, Wang X, Hagfeldt A, Sun L (2007) Effect of tetrahydro-quinoline dyes structure on the performance of organic dye-sensitized solar cells. Chem Mater 19(16):4007–4015
19. Walsh PJ, Gordon KC, Officer DL, Campbell WM (2006) A DFT study of the optical properties of substituted Zn(II) TPP complexes. J Mol Struct (THEOCHEM) 759(1–3):17–24
20. Balanay MP, Kim DH (2009) Structures and excitation energies of Zn-tetraarylporphyrin analogues: A theoretical study. J Mol Struct (THEOCHEM) 910(1–3):20–26
21. De Angelis F, Fantacci S, Mosconi E, Nazeeruddin MK, Grätzel M (2011) Absorption spectra and excited state energy levels of the N719 dye on $TiO_2$ in dye-sensitized solar cell models. J Phys Chem C 115(17):8825–8831
22. Pastore M, Fantacci S, De Angelis F (2010) Ab initio determination of ground and excited state oxidation potentials of organic chromophores for dye-sensitized solar cells. J Phys Chem C 114(51):22742–22750
23. Nishida J, Masuko T, Cui Y, Hara K, Shibuya H, Ihara M, Hosoyama T, Goto R, Mori S, Yamashita Y (2010) Molecular design of organic dye toward retardation of charge recombination at semiconductor/dye/electrolyte interface: Introduction of twisted π-linker. J Phys Chem C 114(41):17920–17925
24. Preat J, Jacquemin D, Perpete E (2010) Design of new triphenylamine-sensitized solar cells: a theoretical approach. Environ Sci Technol 44(14):5666–5671
25. Preat J (2010) Photoinduced energy-transfer and electron-transfer processes in dye-sensitized solar cells: TDDFT insights for triphenylamine dyes. J Phys Chem C 114(51):16716–16725
26. Chidthong R, Hannongbua S (2010) Excited state properties, fluorescence energies, and lifetimes of a poly(fluorene-phenylene), based on TD-DFT investigation. J Comput Chem 31(7):1450–1457
27. Meeto W, Suramit S, Lukeš V, Wolschann P, Hannongbua S (2010) Effects of the CN and $NH_2$ substitutions on the geometrical and optical properties of model vinylfluorenes, based on DFT calculations. J Mol Struct (THEOCHEM) 939(1–3):75–81
28. Baerends EJ, Gritsenko OV (1997) A quantum chemical view of density functional theory. J Phys Chem A 101(30):5383–5403
29. Runge E, Gross EKU (1984) Density-functional theory for time-dependent systems. Phys Rev Lett 52(12):997–1000
30. Dreuw A, Head-Gordon M (2005) Single-reference ab initio methods for the calculation of excited states of large molecules. Chem Rev 105(11):4009–4037
31. Bauernschmitt R, Ahlrichs R (1996) Treatment of electronic excitations within the adiabatic approximation of time dependent density functional theory. Chem Phys Lett 256(4–5):454–464
32. Stratmann RE, Scuseria GE, Frisch MJ (1998) An efficient implementation of time dependent density-functional theory for the calculation of excitation energies of large molecules. J Chem Phys 109(19):8218–8227
33. Perdew JP, Ruzsinszky A, Tao J, Staroverov VN, Scuseria GE, Csonka GI (2005) Prescription for the design and selection of density functional approximations: More constraint satisfaction with fewer fits. J Chem Phys 123(23):062201–062209
34. Adamo C, Barone V (1999) Toward reliable density functional methods without adjustable parameters: the PBE0 model. J Chem Phys 110(13):6158–6169
35. Yanai T, Tew DP, Handy NC (2004) A new hybrid exchange–correlation functional using the Coulomb-attenuating method (CAM-B3LYP). Chem Phys Lett 393(1–3):51–57
36. Aidas K, Møgelhøj A, Nilsson EJK, Johnson MS, Mikkelsen KV, Christiansen O, Söderhjelm P, Kongsted J (2008) On the performance of quantum chemical methods to predict solvatochromic effects: the case of acrolein in aqueous solution. J Chem Phys 128(19):194503–194515
37. Sriwichitkamol K, Suramitr S, Poolmee P, Hannongbua S (2006) Structures, absorption spectra, and electronic properties of polyfluorene and its derivatives: a theoretical study. J Theor Comp Chem 5(3):595–608
38. Becke AD (1988) Density-functional exchange-energy approximation with correct asymptotic behavior. Phys Rev A 38(6):3098–3100
39. Lee C, Yang W, Parr RG (1988) Development of the Colle-Salvetti correlation-energy formula into a functional of the electron density. Phys Rev B 37(2):785–789
40. Becke AD (1993) Density-functional thermochemistry. III. The role of exact exchange. J Chem Phys 98(7):5648–5652
41. Zhao Y, Truhlar DG (2008) The M06 suite of density functionals for main group thermochemistry, thermochemical kinetics, noncovalent interactions, excited states, and transition elements: two new functionals and systematic testing of four M06-class functionals and 12 other functionals. Theor Chem Acc 120(1–3):215–241
42. Zhao Y, Truhlar DG (2008) Density functionals with broad applicability in chemistry. Acc Chem Res 41(2):157–167
43. Møller C, Plesset MS (1934) Note on an approximation treatment for many-electron systems. Phys Rev 46(7):618–622
44. Hehre WJ, Ditchfield R, Pople JA (1972) Self-consistent molecular orbital methods. XII. Further extensions of gaussian-type basis sets for use in molecular orbital studies of organic molecules. J Chem Phys 56(5):2257–2261
45. Frisch MJ, Trucks GW, Schlegel HB, Scuseria GE, Robb MA, Cheeseman JR, Scalmani G, Barone V, Mennucci B, Petersson GA, Nakatsuji H, Caricato M, Li X, Hratchian HP, Izmaylov AF, Bloino J, Zheng G, Sonnenberg JL, Hada M, Ehara M, Toyota K, Fukuda R, Hasegawa J, Ishida M, Nakajima T, Honda, Y, Kitao O, Nakai H, Vreven T, Montgomery Jr JA, Peralta JE, Ogliaro F, Bearpark M, Heyd JJ, Brothers E, Kudin KN, Staroverov VN,

Keith T, Kobayashi R, Normand J, Raghavachari K, Rendell A, Burant JC, Iyengar SS, Tomasi J, Cossi M, Rega N, Millam JM, Klene M, Knox JE, Cross JB, Bakken V, Adamo C, Jaramillo J, Gomperts R, Stratmann RE, Yazyev O, Austin AJ, Cammi R, Pomelli C, Ochterski JW, Martin RL, Morokuma K, Zakrzewski VG, Voth GA, Salvador P, Dannenberg JJ, Dapprich S, Daniels AD, Farkas O, Foresman JB, Ortiz JV, Cioslowski J, Fox DJ (2010) GAUSSIAN09 Rev. B.01., Gaussian Inc.: Wallingford CT

46. Stalmach U, Detert H (2000) Synthesis and electronic spectra of substituted p-distyrylbenzenes for the use in light-emitting diodes. Adv Synth Catal 342(1):10–16
47. Jacquemin D, Femenias A, Chermette H, Andre JM, Perpete EA (2005) Second-order Møller-Plesset evaluation of the bond length alternation of several series of linear oligomers. J Phys Chem A 109(25):5734–5741
48. Jacquemin D, Adamo C (2011) Bond length alternation of conjugated oligomers: wave function and DFT benchmarks. J Chem Theory Comput 7(2):369–376
49. Cai Z-L, Crossley MJ, Reimers JR, Kobayashi R, Amos RD (2006) Density functional theory for charge transfer: The nature of the N-bands of porphyrins and chlorophylls revealed through CAM-B3LYP, CASPT2, and SAC-CI calculations. J Phys Chem B 110(31):15624–15632
50. Peach MJG, Helgaker T, Salek P, Keal TW, Lutnaes OB, Tozer DJ, Handy NC (2006) Assessment of a Coulomb-attenuated exchange-correlation energy functional. Phys Chem Chem Phys 8(5):558–562
51. Krishnan R, Binkley JS, Seeger R, Pople JA (1980) Self-consistent molecular orbital methods. XX. A basis set for correlated wave functions. J Chem Phys 72(1):650–654
52. Suramitr S, Meeto W, Wolschann P, Hannongbua S (2009) Understanding on absorption and fluorescence electronic transitions of carbazole-based conducting polymers: TD-DFT approaches. Theor Chem Acc 125(1):35–44
53. Cramer CJ, Truhlar DG (1999) Implicit solvation models: Equilibria, structure, spectra, and dynamics. Chem Rev 99(8): 2161–2200
54. Cossi M, Barone V (2001) Time-dependent density functional theory for molecules in liquid solutions. J Chem Phys 115(10): 4708–4710
55. Tomasi J, Mennucci B, Cammi R (2005) Quantum mechanical continuum solvation models. Chem Rev 105(8):2999–3094
56. Scalmani G, Frisch MJ, Mennucci B, Tomasi J, Cammi R, Barone V (2006) Geometries and properties of excited states in the gas phase and in solution: theory and application of a time-dependent density functional theory polarizable continuum model. J Chem Phys 124(9):94107–94115
57. Suramitr S, Kerdcharoen T, Srikhirin T, Hannongbua S (2005) Electronic properties of alkoxy derivatives of poly(para-phenylenevinylene), investigated by time-dependent density functional theory calculations. Synth Met 155(1):27–34
58. Grimme S (2011) Density functional theory with London dispersion corrections. Comput Mol Sci 1:211–228
59. Dreuw A, Head-Gordon M, Dreuw A, Head-Gordon M (2004) Failure of time-dependent density functional theory for long-range charge-transfer excited states: The zincbacteriochlorin-bacteriochlorin and bacteriochlorophyll-Spheroidene Complexes. J Am Chem Soc 126(12):4007–4016
60. Jacquemin D, Perpète EA, Scuseria GE, Ciofini I, Adamo C (2008) TD-DFT performance for the visible absorption spectra of organic dyes: conventional versus long-range hybrids. J Chem Theory Comput 4(1):123–135
61. Tawada Y, Tsuneda T, Yanagisawa S, Yanai T, Hirao K (2004) A long-range-corrected time-dependent density functional theory. J Chem Phys 120(18):8425–8433
62. Korth M, Grimme S (2009) "Mindless" DFT benchmarking. J Chem Theory Comput 5(4):993–1003
63. Grimme S, Hujo W, Kirchner B (2012) Performance of dispersion-corrected density functional theory for the interactions in ionic liquids. Phys Chem Chem Phys 14:4875–4883
64. Chai JD, Head-Gordon M (2008) Long-range corrected hybrid density functionals with damped atom–atom dispersion corrections. Phys Chem Chem Phys 10(44):6615–6620
65. Kang YK, Byun BJ (2010) Assessment of density functionals with long-range and/or empirical dispersion corrections for conformational energy calculations of peptides. J Comput Chem 31(16):2915–2923
66. Suramitr S, Phalinyot S, Wolschann P, Fukuda R, Ehara M, Hannongbua S (2012) Photophysical properties and photochemistry of EE-, EZ-, and ZZ-1,4-dimethoxy-2,5-bis[2 (thien-2-yl) ethenyl] benzene in solution: theory and experiment. J Phys Chem A 116(3):924–937
67. Barbara PF, Meyer TJ, Ratner MA (1996) Contemporary issues in electron transfer research. J Phys Chem 100(31):13148–13168
68. Lin BC, Cheng CP, You Z-Q, Hsu C-P (2005) Charge transport properties of tris(8-hydroxy-quinolinato)aluminum(III): why it is an electron transporter. J Am Chem Soc 127(1):66–67
69. Haque SA, Tachibana Y, Willis LR, Moser JE, Grätzel M, Klug DR, Durrant JR (2000) Parameters influencing charge recombination kinetics in dye-sensitized nanocrystalline titanium dioxide films. J Phys Chem B 104(3):538–547
70. Hutchison GR, Ratner MA, Marks TJ (2005) Hopping transport in conductive heterocyclic oligomers: reorganization energies and substituent effects. J Am Chem Soc 127(7):2339–2350
71. García G, Timon V, Hernandez-Laguna A, Navarro A, Fernandez-Gomez M (2011) Influence of the alkyl and alkoxy side chains on the electronic structure and charge-transport properties of polythiophene derivatives. Phys Chem Chem Phys 13(21): 10091–10099
72. Preat J, Michaux C, Jacquemin D, Perpete EA (2009) Enhanced efficiency of organic dye-sensitized solar cells: triphenylamine derivatives. J Phys Chem C 113(38):16821–16833
73. Baik C, Kim D, Kang M-S, Kang SO, Ko J, Nazeeruddin MK, Grätzel M (2009) Organic dyes with a novel anchoring group for dye-sensitized solar cell applications. J Photochem Photobiol A Chem 201(2–3):168–174
74. Hara K, Miyamoto K, Abe Y, Yanagida M (2005) Electron transport in coumarin-dye-sensitized nanocrystalline TiO2 electrodes. J Phys Chem B 109(50):23776–23778
75. Hara K, Kurashige M, Dan-Oh Y, Kasada C, Shinpo A, Suga S, Sayama K, Arakawa H (2003) Design of new coumarin dyes having thiophene moieties for highly efficient organic-dye-sensitized solar cells. New J Chem 27(5):783–785
76. Balanay MP, Dipaling CVP, Lee SH, Kim DH, Lee KH (2007) AM1 molecular screening of novel porphyrin analogues as dye-sensitized solar cells. Sol Energy Mater Sol Cells 91(19):1775–1781